

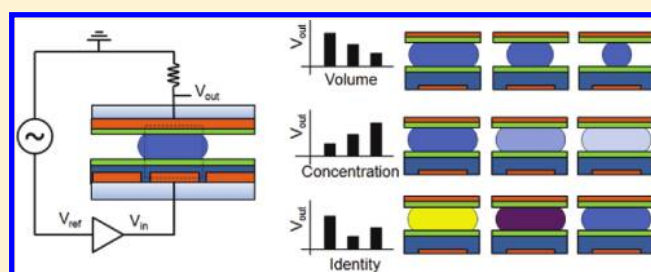
# On Chip Droplet Characterization: A Practical, High-Sensitivity Measurement of Droplet Impedance in Digital Microfluidics

Saman Sadeghi,<sup>†,‡</sup> Huijiang Ding,<sup>†,‡</sup> Gaurav J. Shah,<sup>†,‡</sup> Supin Chen,<sup>§</sup> Pei Yuin Keng,<sup>†,‡</sup> Chang-Jin “CJ” Kim,<sup>⊥</sup> and R. Michael van Dam<sup>\*,†,‡,§</sup>

<sup>†</sup>Department of Molecular and Medical Pharmacology, David Geffen School of Medicine, <sup>‡</sup>Crump Institute for Molecular Imaging, <sup>§</sup>Biomedical Engineering Department, <sup>⊥</sup>Mechanical and Aerospace Engineering Department, University of California, Los Angeles, California, United States

## Supporting Information

**ABSTRACT:** We demonstrate a new approach to impedance measurement on digital microfluidics chips for the purpose of simple, sensitive, and accurate volume and liquid composition measurement. Adding only a single series resistor to existing AC droplet actuation circuits, the platform is simple to implement and has negligible effect on actuation voltage. To accurately measure the complex voltage across the resistor (and hence current through the device and droplet), the designed system is based on software-implemented lock-in amplification detection of the voltage drop across the resistor which filters out noise, enabling high-resolution and low-limit signal recovery. We observe picoliter sensitivity with linear correlation of voltage to volume extending to the microliter volumes that can be handled by digital microfluidic devices. Due to the minimal hardware, the system is robust and measurements are highly repeatable. The detection technique provides both phase and magnitude information of the real-time current flowing through the droplet for a full impedance measurement. The sensitivity and resolution of this platform enables it to distinguish between various liquids which, as demonstrated in this paper, could potentially be extended to quantify solute concentrations, liquid mixtures, and presence of analytes.



There have been tremendous advances in miniaturized analytical systems and microreactors in the past decade, and the promise of a true lab on a chip is close at hand for several chemical synthesis and biosensor applications.<sup>1–5</sup> Many of the technologies introduced build on intrinsic advantages of microfluidic systems such as manipulation of small volumes, deterministic flow profiles, enhanced kinetics, short analysis times, and the overall reduced footprint of the devices.<sup>6,7</sup> Leveraging these capabilities to achieve precise spatial and/or temporal control of concentrations of fluids handled underpins the high performance and novelty of many of these interesting systems.

Droplet-based digital microfluidic platforms, such as those based on electrowetting (e.g., electrowetting-on-dielectric, EWOD)<sup>9,10</sup> and dielectrophoresis (DEP)<sup>11,12</sup> are in many ways ideal for applications where discrete small samples must be reacted or analyzed in a highly flexible manner. Such droplet-based systems present a particular challenge, however, in that practical issues such as evaporation, uneven droplet splitting, or residues resulting from fouled surfaces, can lead to undesired changes in volumes and concentrations over time, especially in systems where droplets are surrounded by air<sup>16</sup> rather than oil.<sup>15</sup> Fortunately, the electromechanical scheme employed in both EWOD and DEP is inherently amenable to integration of electronic detection of liquid properties. By monitoring the capacitance between two electrodes, it is

possible to determine the volume of liquid in the intervening space or even the composition.<sup>13,14</sup> Furthermore, this detection can be used as part of a feedback system to detect and correct for droplet actuation failures<sup>17–19</sup> or facilitate accurate volume measurement and dispensing<sup>20,21</sup> to achieve precise and dynamic control of fluid concentrations.

Ren et al.<sup>20</sup> used an on-chip measurement of volume to control an external mechanical pump to dispense droplets into an EWOD chip. Volume was determined by measuring capacitance in between the EWOD electrodes through frequency modulation of a ring oscillator circuit. Using the same basic measurement approach, Gong et al.<sup>21</sup> demonstrated that precise volumes of droplets can be dispensed by feedback-controlled EWOD actuation directly on chip, i.e., without using any external fluidic system or pump. However, the relatively complex circuitry and the high sampling rates required in this measurement approach limit the applicability in low cost and point of care devices; in addition, this approach is limited to detect capacitance change when the EWOD device is being operated under DC voltage conditions. DC operation severely limits the variety of liquids that can be actuated<sup>22</sup> and increases the chance of dielectric breakdown in the device,<sup>23</sup> which may

Received: October 21, 2011

Accepted: January 16, 2012

Published: January 16, 2012

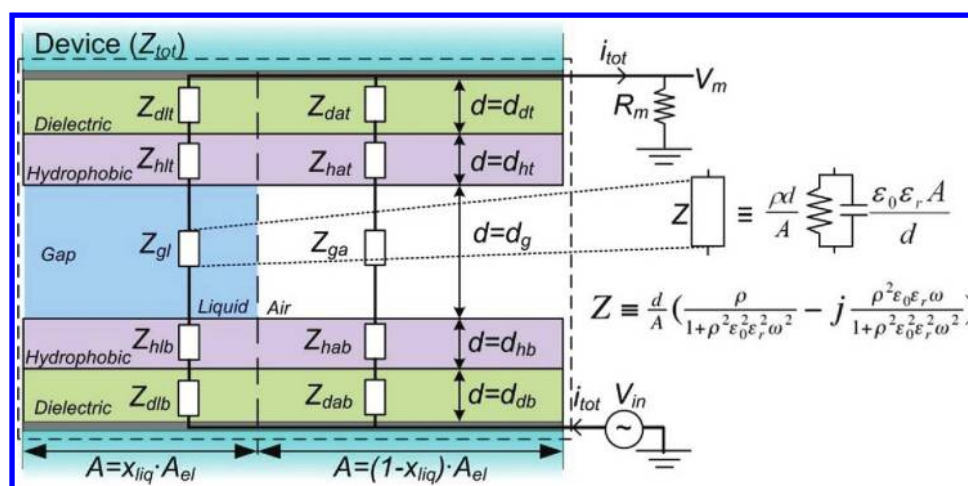


**Figure 1.** (a) Equivalent electrical circuit model for a standard two-plate EWOD device, where a fraction ( $x_{liq}$ ) of the electrode area ( $A_{el}$ ) is covered by the liquid. The circuit can be divided into two parallel branches, one going through the liquid and the other through the surrounding fluid (e.g., air) in the gap. The dielectric (subscript d) and hydrophobic (subscript h) layers on the top (subscript t) and bottom (subscript b) substrates and the liquid (subscript l) and air (subscript a) in the gap can all be represented in general by a complex electrical impedance (white box). (Inset) Each complex impedance  $Z_{xyz}$  consists of a resistor in parallel with a capacitor, calculated using the resistivity and permittivity of each material and its geometry, i.e., the cross sectional area  $A$  and thickness  $d$ . For instance, the liquid impedance would have  $A = A_{el}x_{liq}$  and  $d = d_g$ .

cause irreversible reactions and oxidation in the chip.<sup>24</sup> Furthermore, the accuracy and the resolution are fundamentally limited by the magnitude of the induced frequency shift and ability of the system to resolve high frequency modulations. For example, from the report of Gong et al.,<sup>19</sup> a frequency shift of 1.9 nL/kHz can be approximated when an oscillation frequency of 1–3 MHz is applied. Detecting a 1 kHz shift in a MHz oscillation frequency requires fast sampling rates and sophisticated electronics, and nanoliter resolution would require a waiting time of 2 ms to accurately quantify a 0.5 kHz shift by pulse counting. A simpler, more sensitive device would present significant advantages. Shih et al.<sup>25</sup> have recently proposed an alternative method for detecting capacitive change in digital microfluidic devices based on measuring voltage drop across an external circuit. Although this method simplifies the instrumentation, it relies on the introduction of a large shunt resistor to produce a substantial and measurable potential, which can produce a significant voltage burden on the circuit. The influence of the measuring circuit on the device in this example cannot be ignored, especially for measurement of higher conductivity samples, and as described in the Theoretical section, the phase shift introduced by a large added resistor would not be compatible with an accurate complex value impedance analysis. Nevertheless, this simple device eliminates the need for high frequency electronics and could supply feedback to improve the fidelity of protein and enzymatic assays. Impedance measurement can determine not only volume but also composition of droplets. Schertzer et al. demonstrated the principle of measuring the composition of water–methanol droplets<sup>13</sup> but used an expensive commercial capacitance meter to make measurements, which may not be suitable in many applications.

In this paper, we report an impedance detection technique that further simplifies the required hardware of the Shih et al. approach to a single, small, precision resistor in series with the AC actuation potential applied to the device. The measurement has negligible impact on actuation (e.g., 200 mV drop across the resistor for an applied voltage of 100 V). A low-cost lock-in amplifier<sup>26</sup> (implemented in software) minimizes noise, enabling a detection limit of 10  $\mu$ V. For our device geometry,

the sensing electrode has a capacity of about 300 nL of fluid, corresponding to a limit of detection in the pL volume range. The method additionally provides phase information which helps to distinguish liquids based on differences in their electrical properties.

A theoretical overview of the measurement technique is first described, along with a discussion of the significance of measured variables in the context of droplet volume measurement, liquid identification, and composition analysis. Results of volume measurement, solvent classification, and concentration measurement are then presented and discussed, followed by a demonstration of real-time volume measurements of an evaporating droplet of acetonitrile. This platform could find use in a wide range of applications, such as platforms for handling small volumes of biochemical samples or microfluidic synthesizers for radiotracers, which require precise monitoring and/or control of volumes and compositions.<sup>27,28</sup>

## THEORETICAL

In this section, we lay out a theoretical model to relate the electrical signal to the properties of the volume of space between the sensing electrode and reference electrode in a device having the common parallel plate configuration. In essence, the introduction of the liquid in this volume (initially filled with air or another surrounding medium) changes the complex electrical impedance as a function of the fraction of the sensing volume occupied by the liquid, or the “liquid fraction” ( $x_{liq}$ ), and the electrical properties (resistivity, permittivity) of the liquid. Knowing the relation of this change to the total current ( $i_{tot}$ ) through the device, we can obtain information about the quantity and/or nature of the liquid by accurately measuring  $i_{tot}$ . The equations derived from first principles in this section formulate the relation of the measured signal to droplet volume and identity.

As shown in the simplified schematic of Figure 1a, a droplet partially covering an electrode inside a two-plate EWOD device can be modeled as an electrical circuit by representing each of the dielectric and hydrophobic layers of the device, and the liquid and air in the gap, as complex electrical impedances.<sup>29</sup>

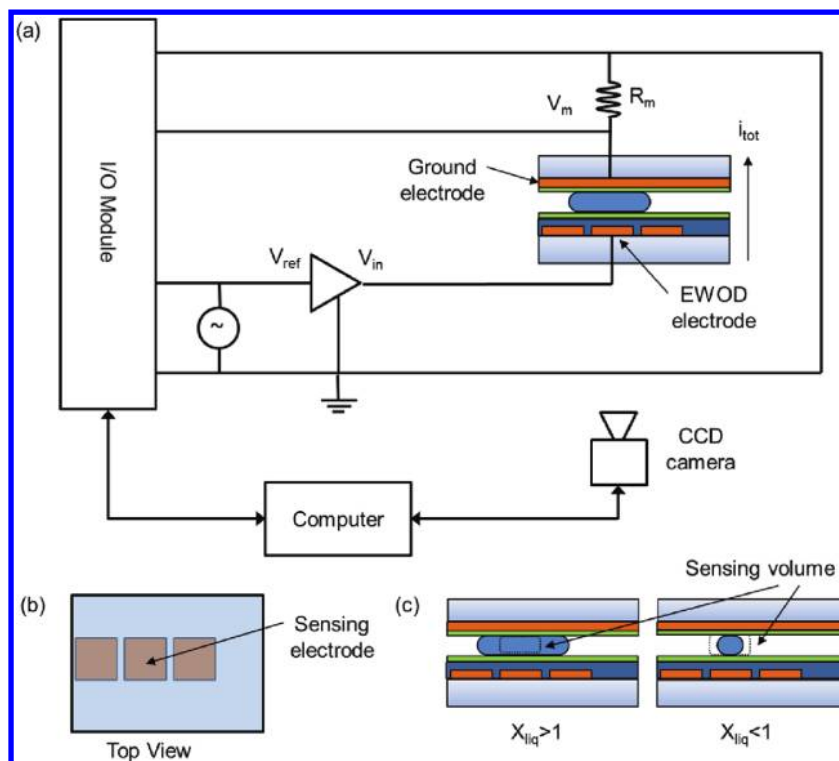


**Figure 2.** Schematic of the liquid detection system. (a) Diagram of the impedance measurement system. (b) Top view of the EWOD chip. (c) Side view of the chip showing sensing volume for the cases where droplet is larger than the electrode ( $x_{liq} > 1$ ) or smaller than the electrode ( $x_{liq} < 1$ ).

Assuming the electric field lines are vertical (i.e., ignoring fringing fields), the circuit can be considered to have parallel branches through the air and the liquid in the gap. A change in the impedance due to introduction of the liquid would change the total device impedance ( $Z_{tot}$ ). For a fixed geometry and material properties of the device layers, the total impedance of the device (considering only this one electrode) is dependent on the electrical properties (relative permittivity ( $\epsilon_r$ ) and resistivity ( $\rho_l$ )) and the liquid fraction ( $x_{liq}$ ). Assuming sidewalls of the droplet are vertical (i.e., contact angle is  $90^\circ$ ), the latter is directly proportional to the liquid volume, while the former depends on the type of liquid, concentration of solutes, etc. The total current  $i_{tot}$  through the device is measured in the form of voltage ( $V_m$ ) across a small measurement resistance ( $R_m$ ) in series with the device, i.e.,  $V_m = i_{tot}R_m$ .

We next examine the relation between the frequency-specific device current to the liquid fraction and the resistivity and permittivity of the liquid. We start by relating each of the complex impedances in the circuit (Figure 1a) to the material properties and geometry. Assuming the thickness to be small compared to the lateral dimensions (which is typical for EWOD chip), each of the impedances can be approximated to be a parallel-plate capacitor in parallel with a resistor of uniform cross-section (Figure 1a inset). For a thickness  $d$  and cross-sectional area  $A$ , the equivalent capacitance and resistance, respectively, are

$$C = \frac{\epsilon_0 \epsilon_r A}{d} \quad R = \frac{\rho d}{A} \quad (1)$$

The complex impedance,  $Z$ , for a capacitor in parallel with a resistor depends on the signal frequency ( $f$ ) and is given by

$$Z = \frac{R - jR^2C\omega}{1 + R^2C^2\omega^2} \quad j = \sqrt{-1}, \quad \omega = 2\pi f \quad (2)$$

Substituting for  $C$  and  $R$  from eq 1 and simplifying, we obtain

$$Z = \frac{d}{A} \left( \frac{\rho}{1 + \rho^2 \epsilon_0^2 \epsilon_r^2 \omega^2} - j \frac{\rho^2 \rho \epsilon_0 \epsilon_r \omega}{1 + \rho^2 \epsilon_0^2 \epsilon_r^2 \omega^2} \right) \quad (3)$$

It should be noted that, in general, both the real and imaginary components of  $Z$  are dependent on the liquid's resistivity as well as permittivity. In addition, both components of  $Z$  are directly proportional to the thickness ( $d$ ) and inversely proportional to the area ( $A$ ). The latter, along with Ohm's law, implies that, for a fixed voltage across the impedance  $V$  and fixed thickness  $d$ , the current  $i$  through this impedance would be linearly proportional to its cross-sectional area  $A$ .

$$\begin{aligned} i &= \frac{V}{Z} \\ &= \frac{VA}{d} \frac{1 + \rho^2 \epsilon_0^2 \epsilon_r^2 \omega^2}{(\rho - j\rho^2 \epsilon_0 \epsilon_r \omega)} \\ &= \frac{VA}{d} \left( \frac{1}{\rho} + j\epsilon_0 \epsilon_r \omega \right) \end{aligned} \quad (4)$$

The total impedance, as depicted in Figure 1, can be visualized as two sets of series impedances in parallel, one for the liquid-containing path and one for the air-containing path, i.e.,  $Z_l = Z_{dl} + Z_{hl} + Z_{gl} + Z_{hlb} + Z_{dlb} = z_l / (x_{liq} A_{el})$  and  $Z_a = Z_{dat} + Z_{hat} + Z_{ga} + Z_{hab} + Z_{dab} = z_a / [(1 - x_{liq}) A_{el}]$ , where  $z_l$  and  $z_a$  are "specific" impedances. The total current can therefore be expressed as

Table 1. Summary of Electrical and Geometrical Parameters Used in Simulation and Experiments<sup>a</sup>

material	resistivity $\rho$ ( $\Omega$ m)	relative permittivity $\epsilon_r$	thickness $d$ ( $\mu$ m)	impedance over entire electrode (4.0 mm <sup>2</sup> ) at $f = 10$ kHz
dielectric, top (Si <sub>3</sub> N <sub>4</sub> ) <sup>30</sup>	$1 \times 10^{10}$	7.0	0.1	$1.7 \times 10^{-1} - 6.4 \times 10^3 j$
hydrophobic, top (Cytop) <sup>1</sup>	$1 \times 10^{15}$	2.0	0.1	$2.0 \times 10^{-5} - 2.2 \times 10^4 j$
dielectric, bottom (Si <sub>3</sub> N <sub>4</sub> )	$1 \times 10^{10}$	7.0	1.0	$1.7 \times 10^0 - 6.4 \times 10^4 j$
hydrophobic, bottom (Cytop)	$1 \times 10^{15}$	2.0	1.0	$2.0 \times 10^{-4} - 2.2 \times 10^5 j$
water <sup>22</sup>	$1.8 \times 10^5$	80.1	75	$5.1 \times 10^4 - 4.2 \times 10^5 j$
dimethyl sulfoxide (DMSO) <sup>22</sup>	$3.3 \times 10^4$	47.2	75	$3.5 \times 10^5 - 3.1 \times 10^5 j$
acetonitrile (MeCN) <sup>22</sup>	$5.2 \times 10^4$	36.6	75	$4.6 \times 10^5 - 4.9 \times 10^5 j$
air <sup>31</sup>	$\sim 2 \times 10^{14}$	1.0	75	$3.0 \times 10^{-1} - 3.4 \times 10^7 j$

<sup>a</sup>The complex impedance for a layer of each material, assuming it spans across the entire electrode area, is also tabulated at a signal frequency of 10 kHz.

$$\begin{aligned}
 i_{tot} &= \frac{V_{in}}{Z_{tot}} \\
 &= V_{in} \frac{Z_l + Z_a}{Z_l Z_a} \\
 &= V_{in} A_{el} \left[ \left( \frac{1}{z_l} - \frac{1}{z_a} \right) x_{liq} + \frac{1}{z_a} \right] \quad (5)
 \end{aligned}$$

which is a linear function of the area fraction of the gap filled with liquid  $x_{liq}$ . Thus, for fixed geometry and liquid properties, the volume of liquid in the sensing region can be estimated from  $V_m$ . For  $x_{liq} = 0$ ,  $i_{tot} = V_{in} A_{el}/z_a$  and for  $x_{liq} = 1$ ,  $i_{tot} = V_{in} A_{el}/z_l$ .

## METHODS

Details of EWOD chip design, hardware setup, optical measurement of droplet size and impedance measurement technique are detailed in the Supporting Information.

**Droplet Impedance Sensing.** The only hardware added for impedance measurement was a single 1 k $\Omega$  precision series resistor in the path of the current from the cover plate to the ground of the amplifier (Figure 2). In comparison to the >M $\Omega$  impedance of the EWOD system, containing the droplet under investigation, the monitoring resistor introduces negligible voltage drop and is effectively invisible, meaning the effective voltage available for EWOD actuation is very close to the applied potential  $V_m$ . To make a measurement, the sensing electrode is activated with an AC signal and the voltage  $V_m$  across the 1 k $\Omega$  resistor is monitored. The system requires no additional signal generation for measurement, as the AC potential normally used for EWOD actuation can be used. Just as electrodes can be individually addressed for EWOD actuation, any electrode can be used for sensing. Sensing is thus spatially resolved and reflects the impedance of the particular electrode(s) where EWOD actuation is active, even if multiple droplets are present in the chip. Simultaneous measurements of multiple droplets, though not shown here, could be achieved by addition of a resistor in the individual current path of each electrode before a common ground. The impedance measurement is performed at a single frequency and phase, which allows complete filtering of noise outside of a very narrow frequency band, effectively eliminating noise and affording measurement accuracy down to subnanoliter range.

The signal  $V_{ref}$  from the waveform generator, before amplification for EWOD actuation, was directly monitored by the 16bit data-acquisition card (NI USB-6259, National Instruments) through a differential measurement making use of two analog inputs sampling at 100 kHz. The same

differential measurement was used to acquire the voltage waveform across the shunt resistor (see Figure 2). Because the resistor value is known, this signal represents the current through the device and droplet.

The frequency and phase of the digitized reference signal were measured through a software implementation of phase locked loop (PLL; Figure S1, Supporting Information). The PLL created an internal complex waveform used as a reference to mix with the digitized current measurement passing through the EWOD device. A minimum of 10 cycles of the generated signal (i.e., 1 ms acquisition time from 10 kHz signal; 100 samples at 100 kHz sampling rate) was used for the PLL reference reconstruction. The length of signal used for internal reference was adjusted on the basis of a trade-off between resolution and system response time. The internally generated reference signal was mixed to demodulate the measured current waveform, and a very narrow, first-order finite impulse response (FIR) low pass filter, which introduced negligible phase shift and noise in the reported complex signal, was applied at 5 Hz to extract the component of the measured waveform at the reference frequency. In this way, we were able to measure the phase and the amplitude of the EWOD current at the actuation frequency.

## RESULTS AND DISCUSSION

**Simulations.** MATLAB simulations based on the theoretical model were performed to provide a better understanding of the correlation of the volume, the electrical properties of the liquid in the device, and the voltage measured across the measurement resistance. The theoretical results provided the basis for a set of experiments discussed in the next section to validate the model and to demonstrate the practical applications of the device.

The electrical and geometrical parameters used in the simulation of an EWOD electrode are tabulated in Table 1.

An input voltage of  $V_{in} = 100 \sin(2\pi f)t$  V at  $f = 10$  kHz is applied to the sensing electrode, modeled as shown in Figure 1a. Under these conditions and for a typical EWOD electrode size (2.0 mm  $\times$  2.0 mm), the complex impedance of each of the layers is calculated and presented in the last column of Table 1. It is worth noting that a much lower value of one of the complex components (e.g., real) of  $Z$  implies that the other (reactive, not resistive) component dominates the characteristics of the impedance. For instance, the low real and much higher imaginary part in the case of air, dielectric, and hydrophobic layers implies a very large resistor in parallel with the capacitor. Current passing through such a layer would therefore be approximately 90° out of phase from the voltage across the device. On the other hand, the nearly equal

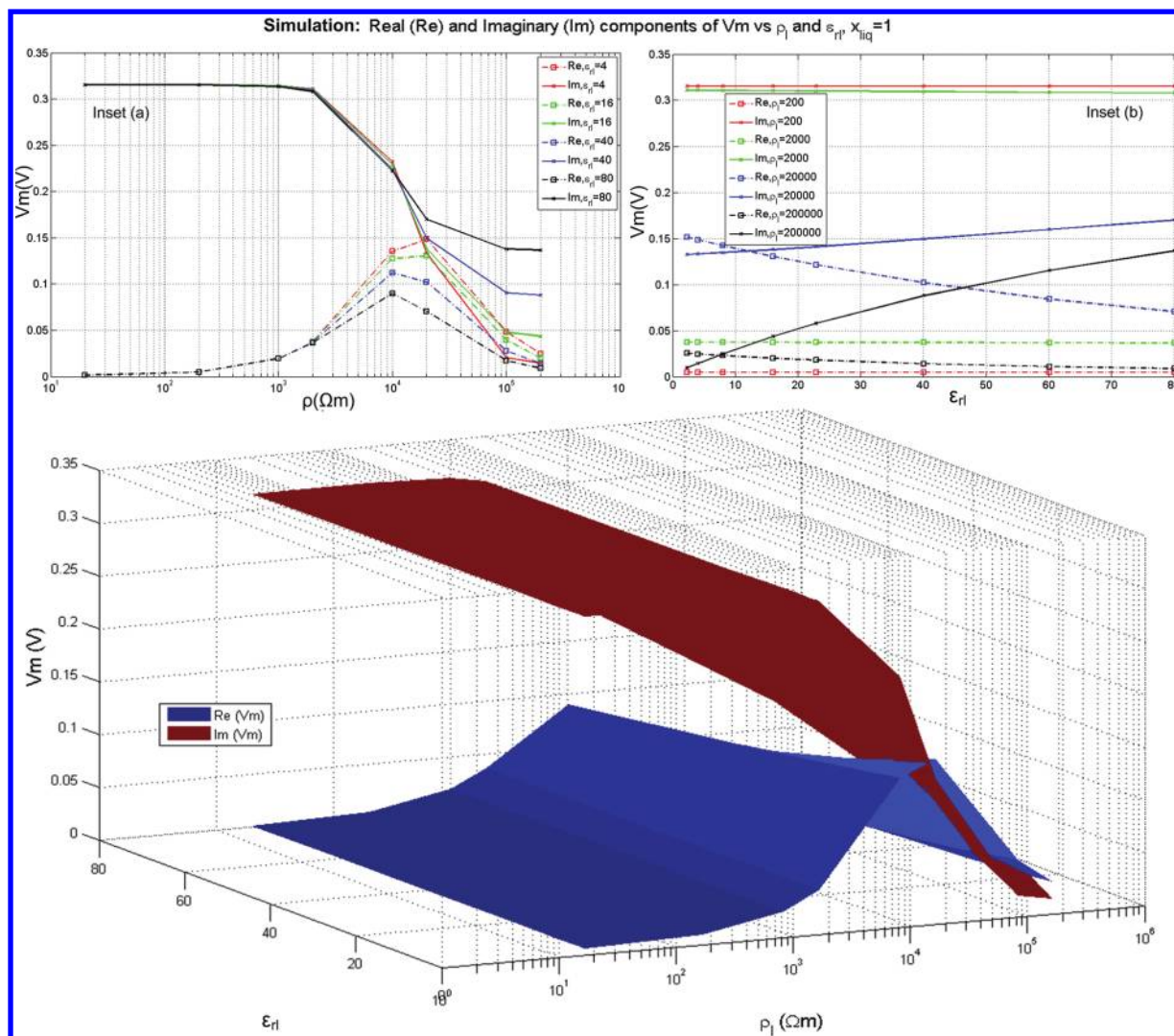


**Figure 3.** Simulated surface plots of the real (blue) and imaginary (red) components of measured voltage  $V_m$  vs the liquid resistivity  $\rho$  and relative permittivity  $\epsilon_r$ . The real component  $\text{Re}\{V_m\}$ , in phase with the input voltage  $V_{in}$ , is bitonic with respect to liquid resistivity  $\rho_l$  but monotonic with respect to liquid's relative permittivity  $\epsilon_r$  while the imaginary component  $\text{Im}\{V_m\}$ , out of phase with the input voltage  $V_{in}$ , is monotonic with respect to both  $\rho_l$  and  $\epsilon_r$ . For greater clarity, 2-D plots for  $V_m$  vs  $\rho_l$  and  $V_m$  vs  $\epsilon_r$  are plotted as insets a and b, respectively, for increasing values of  $\rho_l$  and  $\epsilon_r$ , respectively (red, green, blue, and black in ascending order). The squares and dashed lines represent  $\text{Re}\{V_m\}$ , while  $\times$  and solid lines represent  $\text{Im}\{V_m\}$ . The plots are further discussed in the Supporting Information.

components in case of liquids means that neither of the two terms in eq 3 can be ignored. Changes in resistivity and/or permittivity will affect both the terms and, hence, both real and imaginary parts of the current.

Total current  $i_{tot}$  through the device is measured by monitoring the voltage  $V_m$  across a small measurement resistor  $R_m$ . The real and imaginary components of  $i_{tot}$  and  $V_m$  are, respectively, the in-phase and out-of-phase measured signals with respect to  $V_{in}$ . A detailed discussion of simulations of the influence of parameters like liquid fraction, liquid resistivity, and relative permittivity on the real and imaginary components of  $V_m$  is included in the Supporting Information. The theoretical understanding of the influence of liquid properties on measured complex values of current will allow design of experiments to quantify these properties. The main conclusions from these simulations are as follows: (1) Both real and imaginary components of  $V_m$  are linearly proportional to  $x_{liq}$  for  $x_{liq} \leq 1$ . (2) For known  $x_{liq}$ , both the real and imaginary parts of  $V_m$  are in general a function of the resistivity ( $\rho_l$ ) and relative

permittivity ( $\epsilon_r$ ) of the liquid. Since only the gap impedance varies with these liquid properties, while the other impedances in series do not, the total current through the device (and hence  $V_m$ ) has a nonlinear relationship with  $\rho_l$  and  $\epsilon_r$ . Figure 3 illustrates the variation of  $V_m$  with each of these parameters (for  $x_{liq} = 1$ ). (3)  $\rho_l$  and  $\epsilon_r$  can serve as the “electrical signatures” to identify pure liquids and mixtures of liquids and/or concentrations of solutes in solutions. As compared to purely capacitive sensing (e.g. see ref 32), complex impedance sensing can be much more effective in liquid identification by providing two data-points ( $\text{Re}\{V_{m1}\}$ ,  $\text{Im}\{V_{m1}\}$ ) to identify the two parameters ( $\rho_l$  and  $\epsilon_r$ ) of the liquid.

## EXPERIMENTS

**Measurements of Droplet Size.** Electrical measurements of  $V_m$  and optical measurements of droplet size were obtained for a series of droplet volumes by monitoring a droplet of acetonitrile (MeCN) evaporating at room temperature and were plotted in Figure 4. Consistent with the theoretical

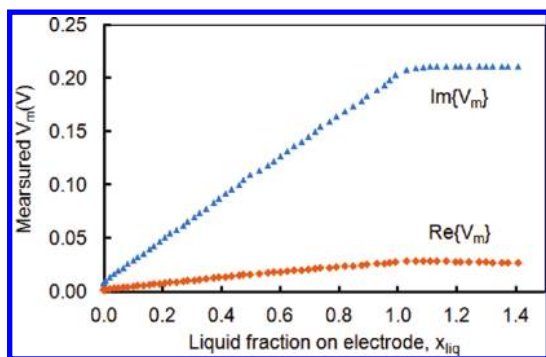


**Figure 4.** Experimental relationship between MeCN liquid fraction  $x_{liq}$  and measured signal  $V_m$ . Real and imaginary components of the measured voltage are shown.

predictions of eq 5 and Figure S2 (Supporting Information), the real and imaginary components of the voltage vary linearly with droplet size in the range  $0 \leq x_{liq} \leq 1$ . For  $x_{liq} > 1$ , the imaginary values remain substantially constant. The real component decreases slightly as the liquid fraction becomes larger than the electrode; this behavior can be attributed to the deviations from ideality which can be anticipated with the EWOD device as pointed out in the previous section or due to increasing parasitic capacitance as the liquid covers larger portions of connection lines from chip edge to the EWOD electrode. In the linear region, one could calibrate the system to read out droplet volume for a droplet of known liquid properties.

For a given value of  $x_{liq}$ , the imaginary part of the measured signal is significantly greater than the real part. This is consistent with theoretical predictions using combinations of dielectric constant and resistivity corresponding to MeCN. As the imaginary part is more sensitive than the real part to  $x_{liq}$  and does not appear to be affected by increasing droplet size above  $x_{liq} = 1$ , the imaginary component is therefore superior for electrically measuring the droplet volume. In most of the subsequent experiments,  $\text{Im}\{V_m\}$  is used.

Within experimental error,  $\text{Im}\{V_m\}$  appears to be linear down to the regime of extremely small droplet size. Multiple measurements were made on a dry electrode over the course of 1 h both before and after an acetonitrile droplet was introduced on the chip. The dry  $\text{Im}\{V_m\}$  signal was found to be  $2.31 \pm 0.01$  mV ( $n = 4$ ). Using a linear fit of Figure 4 to obtain a slope of 0.20 V (or 0.71 V/ $\mu\text{L}$  assuming droplet volume of 280 nL for  $x_{liq} = 1$ ) and  $3\times$  standard deviation of the dry electrode, a limit of detection of 42 pL was estimated for volume measurement. At small droplet sizes (i.e., for small  $x_{liq}$ ), some deviation from linearity is expected in these data due to the presumed slight nonverticality of the droplet walls, the effect of which becomes an increasingly large fraction of the overall droplet volume. In addition, the assumption of parallel plate capacitors used in the Theoretical section breaks down. Furthermore, there is likely a point at which the droplet becomes so small as to detach from one surface of the two plates. This is presumed to happen for droplets with diameter on the order of the gap thickness (i.e., droplet height) or smaller. If this occurs, the optical measurement is not accurate. It is not clear whether the electrical signal continues to be proportional to actual volume of liquid in this regime. At large droplet sizes, however, we were able to repeatedly achieve a linear fit for  $\text{Im}\{V_m\}$  versus volume. Linearity was observed up to a droplet size corresponding to the full volume above the sensing electrode.

**Measurement of Different Liquids.** Since the model predicts a dependence of signal on the permittivity  $\epsilon_r$  and resistivity  $\rho$ . For a fixed volume of fluid, the in-phase (real) and out-of-phase (imaginary) components of the measured signal with respect to the input signal could in principle be used to determine these two electrical properties and hence identify a liquid. In practice, the uncertainties in the dielectric and hydrophobic layers' material properties and thicknesses limit the accuracy of the theoretical model and plots such as Figure 3. Nonetheless,  $\text{Im}\{V_m\}$  and  $\text{Re}\{V_m\}$  can still be used to *classify* liquids.

Signal measurement performed on the same electrode in the same chip, as a function of droplet volume (determined via optical imaging) for different liquids (DMSO and water), is shown in Figure 5. While each liquid maintains the linear

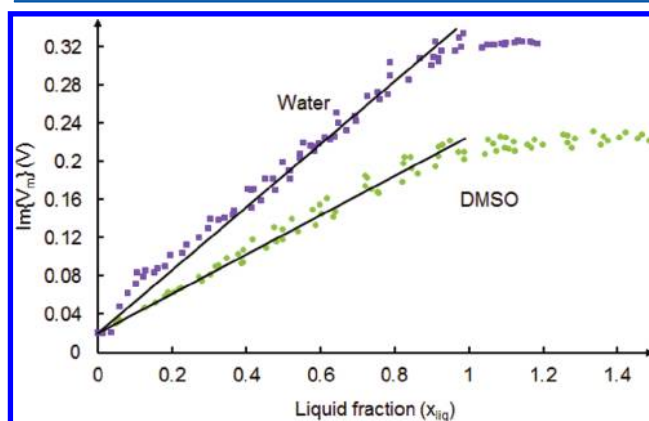


**Figure 5.** Relationship between  $\text{Im}\{V_m\}$  and droplet size ( $x_{liq}$ ) for water and DMSO.

relationship of volume to measured voltage described previously, the distinct slope of each trace is related to the electrical properties of the corresponding liquid. Additional solvents were found to be distinguishable from one another (see Table S1 in the Supporting Information).

**Measurement of Different Salt Concentrations.** The permittivity  $\epsilon_r$  and resistivity  $\rho$  of any solvent are dependent and influenced by the presence of impurities and ionic species. In this way, impedance measurement from the device can be used to quantify salt concentration in the solution. Multiple measurements performed at different concentrations of potassium fluoride (KF) in water showed a clear change in the impedance and a correlation with both real and imaginary components of the measured signal (Figure 6). Measurements exhibited low noise, with small relative standard deviation ( $<0.4\%$ ) observed in multiple measurements of the same droplet (10 samples per second over  $\sim 1$  min; see Figure S4 of Supporting Information).

**Application of Measurement to Monitoring Temporal Dynamics of Evaporating Droplet.** As discussed above, the impedance measurements provide a method to determine the exact volume of a droplet with a single measurement if the fluid properties are known or a calibration plot has been made. For an unknown liquid, relative volume changes can still be acquired, since both  $\text{Re}\{V_m\}$  and  $\text{Im}\{V_m\}$  vary linearly with volume.

In Figure 7, we show the time course of an evaporation of a MeCN droplet at room temperature. Such monitoring has numerous applications, including study of dynamics of

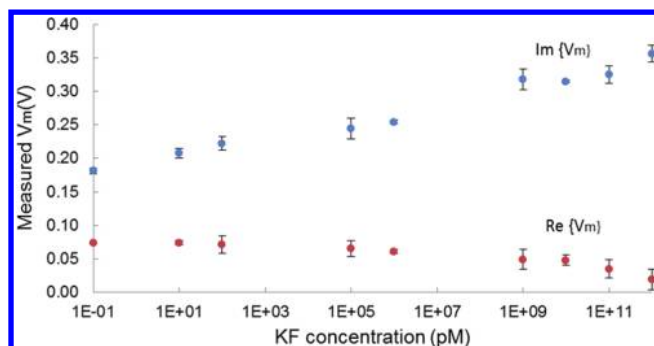


**Figure 6.** Measured signal  $V_m$  with 100 V<sub>rms</sub> excitation potential at 10 kHz, for different concentrations of potassium fluoride (KF) in water. Due to the change in resistivity and permittivity from the dissolved KF, the liquid impedance changes, leading to a change in the total device current, as measured by the change in both real (red) and imaginary (blue) components of the measured signal.

evaporating droplets, measurement of droplet volume during chemical or biochemical processes to monitor concentration, feedback control of size of volatile droplets by providing signal of when to replenish the droplet, etc. Note that fluid properties can be strongly temperature dependent so this would have to be taken into account when making measurements at elevated temperatures where significant temperature gradients could exist.

## CONCLUSIONS

We have introduced and demonstrated a new microfluidic platform for high precision measurement of liquid volume and properties based on impedance measurement from an EWOD device. This simple and robust design adds a single resistor onto the existing EWOD platforms, and its minimal resistance

makes it virtually invisible; thereby, it does not affect the EWOD chip droplet operations such as droplet generation, splitting, and transport. Impedance is determined by measurement of complex voltage over the resistor which is linearly related to the complex current through the device (and droplet). Applying a very narrow bandwidth filter to the output of a digital lock-in amplifier, the device offers excellent detection resolution and the phase information provides an added dimension of information to characterize droplets. Though a DAQ and personal computer were used here, the lock-in amplifier could instead be implemented in hardware such as field programmable gate arrays (FPGAs)<sup>33</sup> for a truly portable device.

We have described a theoretical model for the reported measurement technique, which predicts linear dependence of both the real and imaginary components of the complex measured voltage to the volume of liquid on the sensing electrode. Experimental data shown in this paper is consistent with this linear sensitivity with a dynamic range of volume detection that spans a sensing electrode coverage fraction from 0 to 1 and a limit of detection of 42 pL. Furthermore, through a theoretical discussion of the dependence of liquid properties, namely, resistivity and permittivity, we have described how the device might be used for liquid classification and demonstrated experimentally the distinction of different solvents. These liquid properties are highly sensitive to concentration and composition changes in the liquid (e.g., different salt concentrations), and as such, the device can be used to identify concentration of liquids in an EWOD device and potentially control it through feedback mechanisms. The excellent temporal resolution of the device ( $\sim 1$  ms, as described here) can be used to monitor droplet characteristics in real-time. As an example, we used the system to monitor evaporation dynamics of a volatile

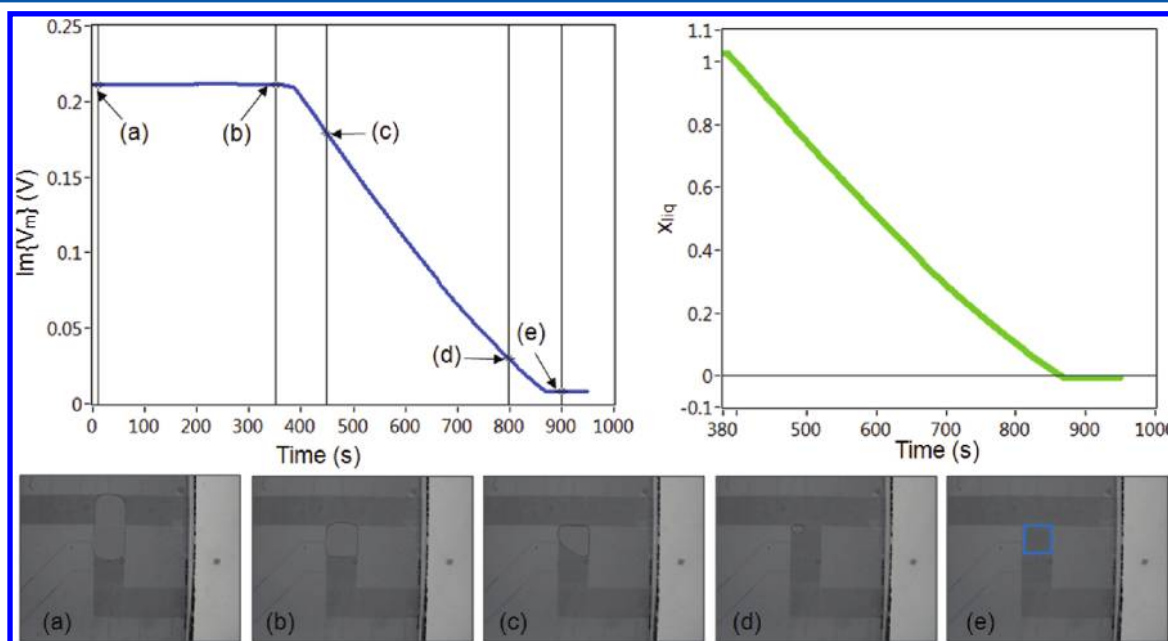


**Figure 7.** Temporal evolution of MeCN droplet size on a 2 mm  $\times$  2 mm electrode at room temperature can be used to study evaporation dynamics. (Left) Temporal evolution of  $V_m$ . (Right) Temporal evolution of droplet size (expressed as  $x_{liq}$ ) as converted by the plot of Figure 4. The flat region (a,b) is when the droplet size is bigger than the sensing electrode. The droplet is smaller than the electrode in the decreasing region (c,d), and is completely evaporated at (e). Since the free surface area of the shrinking droplet decreases over time, the evaporation rate is not linear with time. The bottom figures show optical micrographs of the droplet configuration at the times corresponding to a–e as labeled in the graph. The boundary of the sensing electrode is outlined in the final image.

acetonitrile droplet. Incorporating feedback could allow compensation for changes in volume and concentration through adding more solvent.<sup>34</sup>

The device has been developed on a flexible platform, and several control variables may be adjusted for optimal detection. For example, an increase in operating frequency will linearly increase the signal-to-noise ratio as outlined in the Theoretical section, but this gain may be at the expense of requiring faster sampling rate and more expensive hardware to ensure Nyquist criteria are met and the waveform is digitized with high fidelity. Increasing the electrode area will likewise produce a larger signal, at the expense of increasing the sample volume. Another possible adjustment is the balance between response time and detection accuracy. The length of signal digitized before analysis and the time constant of the software-implemented low pass filter define the level of noise in the signal and the ability to lock into a particular frequency within a narrow band. These control parameters are a measure of flexibility that enable the user to adapt the detection method to the requirements of the experiment which may demand high speed, real-time analysis, or high resolution and sensitivity. As implemented here, sensing can be performed at any site by actuating the EWOD electrode at that site. Calibration need only be performed at any one of these electrode sites, assuming all electrodes are the same size (see Supporting Information). It may be desirable to extend this platform to enable simultaneously sensing at one site and actuation at another location. To do so, one could use different frequency signals for EWOD actuation and impedance sensing. The lock-in detection would then extract the appropriate frequency component, even though the total current through all actuating and sensing electrodes flows through a common ground. This approach could alternatively afford a means to perform sensing at multiple electrodes simultaneously.

The real-time liquid sensing system was used to record the evaporation rate of a volatile organic solvent (acetonitrile) loaded into the EWOD chip which finds application during azeotropic drying of radioactive fluoride ions in the synthesis of [<sup>18</sup>F]FDG on EWOD for positron emission tomography (PET) studies.<sup>28,35</sup> Impedance sensing could potentially be used for *in situ* monitoring of several aspects of the chemical synthesis process and perhaps better control of conditions through feedback mechanisms. The sensitivity and the resolution of the device for changes in the resistivity and permittivity of the droplet may allow for the detection of biological molecules and analytes of interest on an EWOD platform. Leveraging the many advantages of digital microfluidics that have been reported in the literature for biomolecule processing and detection,<sup>36–41</sup> the system described here would open a new and practical avenue for integrating simple, robust, and sensitive biosensors in microfluidic devices.

## ■ ASSOCIATED CONTENT

### ● Supporting Information

Additional information as noted in text. This material is available free of charge via the Internet at <http://pubs.acs.org>.

## ■ AUTHOR INFORMATION

### Corresponding Author

\*E-mail: [mvandam@mednet.ucla.edu](mailto:mvandam@mednet.ucla.edu).

### Notes

The authors declare no competing financial interest.

## ■ ACKNOWLEDGMENTS

This work was funded in part by the University of California Cancer Research Coordinating Committee, the Department of Energy Office of Biological and Environmental Research (DE-SC0001249, DE-SC0005056), and the UCLA Foundation from a donation made by Ralph and Marjorie Crump for the UCLA Crump Institute for Molecular Imaging. The authors greatly appreciate the electronic designs and instrumentation help of Robert W. Silverman.

## ■ REFERENCES

- (1) Hong, J. W.; Quake, S. R. *Nat. Biotechnol.* **2003**, *21*, 1179–1183.
- (2) Weigl, B.; Domingo, G.; LaBarre, P.; Gerlach, J. *Lab Chip* **2008**, *8*, 1999.
- (3) Liu, Y.-J.; Yao, D.-J.; Lin, H.-C.; Chang, W.-Y.; Chang, H.-Y. *J. Micromech. Microeng.* **2008**, *18*, 045017.
- (4) Sun, J.; Masterman-Smith, M. D.; Graham, N. A.; Jiao, J.; Mottahedeh, J.; Laks, D. R.; Ohashi, M.; DeJesus, J.; Kamei, K.-i.; Lee, K.-B.; Wang, H.; Yu, Z. T. F.; Lu, Yi-T.; Hou, S.; Li, K.; Liu, M.; Zhang, N.; Wang, S.; Angenieux, B.; Panosyan, E.; Samuels, E. R.; Park, J.; Williams, D.; Konkankit, V.; Nathanson, D.; van Dam, R. M.; Phelps, M. E.; Wu, H.; Liau, L. M.; Mischel, P. S.; Lazareff, J. A.; Kornblum, H. L.; Yong, W. H.; Graeber, T. G.; Tseng, H.-R. *Cancer Res.* **2010**, *70*, 6128–6138.
- (5) van Dam, R. M.; Elizarov, A. M.; Ball, E.; Shen, C.-F.; Kolb, H.; Rolland, J.; Diener, L.; Williams, D.; Edgcombe, B.; Stephen, T.; Heath, J. R. In *Technical Proceedings of the 2007 NSTI Nanotechnology Conference and Trade Show*, Nano Science and Technology Institute, Cambridge, MA, USA, Santa Clara, CA, May 20–24, 2007; Vol. 3, pp 300–303.
- (6) Mark, D.; Haeberle, S.; Roth, G.; Stetten, F. von; Zengerle, R. *Chem. Soc. Rev.* **2010**, *39*, 1153–1182.
- (7) Squires, T. M.; Quake, S. R. *Rev. Mod. Phys.* **2005**, *77*, 977.
- (8) Whitesides, G. M. *Nature* **2006**, *442*, 368–373.
- (9) Fair, R. *Microfluid. Nanofluid.* **2007**, *3*, 245–281.
- (10) Lee, J.; Moon, H.; Fowler, J.; Schoellhammer, T.; Kim, C.-J. *Sens. Actuators, A: Phys.* **2002**, *95*, 259–268.
- (11) Gascoyne, P. R. C.; Vykoukal, J. V. *Proc. IEEE* **2004**, *92*, 22–42.
- (12) Jones, T. B.; Gunji, M.; Washizu, M.; Feldman, M. J. *J. Appl. Phys.* **2001**, *89*, 1441.
- (13) Schertzer, M. J.; Ben-Mrad, R.; Sullivan, P. E. *Sens. Actuators, B* **2010**, *145*, 340–347.
- (14) Demori, M.; Ferrari, V.; Poesio, P. *Procedia Eng.* **2010**, *5*, 408–411.
- (15) Lin, Y.-Y.; Evans, R. D.; Welch, E.; Hsu, B.-N.; Madison, A. C.; Fair, R. B. *Sens. Actuators, B* **2010**, *150*, 465–470.
- (16) Moon, H.; Cho, S. K.; Garrell, R. L.; Kim, C.-J. *J. Appl. Phys.* **2002**, *92*, 4080.
- (17) Su, F.; Ozev, S.; Chakrabarty, K. *ACM Trans. Des. Autom. Electron. Syst.* **2006**, *11*, 442–464.
- (18) Su, F.; Ozev, S.; Chakrabarty, K. *IEEE Sens. J.* **2005**, *5*, 763–773.
- (19) Gong, J.; Fan, S.-K.; Jin, C.; Kim, C.-J. In *Micro Electro Mechanical Systems; 17th IEEE International Conference on MEMS*; Institute of Electrical and Electronics Engineers (IEEE), New York, NY, 2004; pp 355–358.
- (20) Ren, H.; Fair, R. B.; Pollack, M. G. *Sens. Actuators, B* **2004**, *98*, 319–327.
- (21) Gong, J.; Kim, C.-J. *Lab Chip* **2008**, *8*, 898–906.
- (22) Chatterjee, D.; Hetayothin, B.; Wheeler, A. R.; King, D. J.; Garrell, R. L. *Lab Chip* **2006**, *6*, 199–206.
- (23) Fair, R. B. *Microfluid. Nanofluid.* **2007**, *3*, 245–281.
- (24) Stone, H. A.; Stroock, A. D.; Ajdari, A. *Annu. Rev. Fluid Mech.* **2004**, *36*, 381–411.
- (25) Shih, S. C. C.; Fobel, R.; Kumar, P.; Wheeler, A. R. *Lab Chip* **2011**, *11*, 535–540.
- (26) Cheran, L.-E.; Sadeghi, S.; Thompson, M. *Analyst* **2005**, *130*, 1569.

(27) Sadeghi, S.; Ly, J.; Deng, Y.; van Dam, R. M. In *Proceedings of the Fourteenth International Conference on Miniaturized Systems for Chemistry and Life Sciences*, Curran Associates, Inc., Red Hook, NY, Groningen, The Netherlands, October 3–7, 2010.

(28) Keng, P. Y.; Chen, S.; Ding, H.-J.; Sadeghi, S.; Phelps, M. E.; Satyamurthy, N.; Kim, C.-J.; van Dam, R. M. In *Proceedings of the Fourteenth International Conference on Miniaturized Systems for Chemistry and Life Sciences*, Curran Associates, Inc., Red Hook, NY, Groningen, The Netherlands, October 3–7, 2010.

(29) Jones, T. B.; Wang, K. L.; Yao, D. J. *Langmuir* **2004**, *20*, 2813–2818.

(30) Piccirillo, A. J. *Electrochem. Soc.* **1990**, *137*, 3910.

(31) Pawar, S. D.; Murugavel, P.; Lal, D. M. *J. Geophys. Res.* **2009**, *114*, 8.

(32) Ren, H.; Fair, R. B.; Pollack, M. G. *Sens. Actuators, B* **2004**, *98*, 319–327.

(33) Restelli, A.; Abbiati, R.; Geraci, A. *Rev. Sci. Instrum.* **2005**, *76*, 093112.

(34) Shah, G. J.; Ding, H.; Sadeghi, S.; Chen, S.; Kim, C.-J.; van Dam, R. M. In *16th International Conference on Solid-State Sensors, Actuators and Microsystems*; Institute of Electrical and Electronics Engineers (IEEE), New York, NY, Beijing, China, June 6–9, 2011.

(35) Keng, P. Y.; Chen, S.; Sadeghi, S.; Shah, G. J.; Dooraghi, A.; Phelps, M.; Satyamurthy, N.; Chatziioannou, A. F.; Kim, C.-J.; van Dam, R. M. *Proc. Natl. Acad. Sci. U.S.A.* **2012**, *109*, 690–695.

(36) Luk, V. N.; Wheeler, A. R. *Anal. Chem.* **2009**, *81*, 4524–4530.

(37) Wheeler, A. R.; Moon, H.; Bird, C. A.; Ogorzalek Loo, R. R.; Kim, C.-J.; Loo, J. A.; Garrell, R. L. *Anal. Chem.* **2005**, *77*, 534–540.

(38) Chatterjee, D.; Ytterberg, A. J.; Son, S. U.; Loo, J. A.; Garrell, R. L. *Anal. Chem.* **2010**, *82*, 2095–2101.

(39) Hua, Z.; Rouse, J. L.; Eckhardt, A. E.; Srinivasan, V.; Pamula, V. K.; Schell, W. A.; Benton, J. L.; Mitchell, T. G.; Pollack, M. G. *Anal. Chem.* **2010**, *82*, 2310–2316.

(40) Malic, L.; Veres, T.; Tabrizian, M. *Biosens. Bioelectron.* **2011**, *26*, 2053–2059.

(41) Yoon, J.-Y.; Garrell, R. L. *Anal. Chem.* **2003**, *75*, 5097–5102.